Magnetic Resonance in Medicine 58:144–155 (2007)

Modeling Pulsed Magnetization Transfer

Sharon Portnoy[1] and Greg J. Stanisz[1,2]*

Modeling the effects of clinical magnetization transfer (MT) scans, which generate contrast using short, shaped radiofrequency (RF) pulses (pulsed MT), is complex and time-consuming. As a result, several studies have proposed approximate methods for a simplified analysis of the experimental data. However, potential differences in the MT parameters estimated by each method may complicate the comparison of reported results. In this study we evaluated three approximate methods currently used in quantitative MT (qMT) studies. In the first part of the investigation, an MT modeling technique that makes minimal approximations, other than the use of a two-pool tissue representation, was developed and validated. Subsequently, this technique served as a standard against which to evaluate the other, more approximate models. Each model was used to fit experimental data from samples of wild-type (WT) and *shiverer* mouse spinal cord, as well as simulated data generated by our minimal approximation modeling technique. The results of this study demonstrate that the approximations used in pulsed MT modeling are quite robust. In particular, it was shown that the semisolid pool fraction, M_0^B, which is known to correlate strongly with myelin content, and the transverse relaxation time of macromolecular protons, T_2^B, could be evaluated with reasonable accuracy regardless of the model used. Magn Reson Med 58:144–155, 2007. © 2007 Wiley-Liss, Inc.

Key words: quantitative MRI; magnetization transfer; pulsed MT; continuous wave MT; white matter; spinal cord

Magnetization transfer (MT) is a magnetic resonance imaging (MRI) technique that generates contrast based on the exchange of magnetization between macromolecular and water protons. Unlike other contrast mechanisms (such as longitudinal, T_1, and transverse, T_2, relaxation times), MT provides quantifiable information about the macromolecular components of tissue (proteins, lipids, and cell membranes), which are invisible under normal circumstances due to their short ($\sim$10 μs) T_2 decay constants (1). Both in vivo and in vitro evidence suggests that MT is sensitive to various pathological processes that occur in white matter (WM), including inflammation, demyelination, and axonal loss (2–7). As such, MT is one of the most extensively applied MR-based techniques in the assessment of central nervous system (CNS) disorders (8).

The majority of MT experiments apply an off-resonance radiofrequency (RF) pulse that preferentially saturates the macromolecular magnetization. Subsequently the MR images show a decrease in signal intensity as water protons transfer magnetization to the saturated macromolecules. MT effects in tissues are typically reported in terms of MT ratio (MTR) images, which provide maps of the percent decrease in the MRI signal caused by the MT saturation pulse (5). The MTR, however, reflects a complex combination of biological and experimental parameters, which makes it difficult to attribute any changes to a specific pathological process (7,9). Furthermore, the dependence on experimental parameters makes it difficult to compare MTR findings obtained at different institutions with different protocols (10).

To overcome these limitations, several studies have used a more rigorous quantitative approach that accounts for all of the experimental and biological parameters involved. Such quantitative MT (qMT) experiments have been successfully performed in vitro (2,3,11) and more recently have been applied to human imaging (12–14). qMT techniques achieve greater pathological specificity by determining the physical properties that govern the MT process. These properties include the rate of MT exchange, the transverse and longitudinal relaxation times of water and macromolecular protons, and the relative number of macromolecular protons.

The analysis of qMT data is most commonly based on the two-pool model, which divides the spins within a biological tissue into two pools: 1) a liquid pool composed of water protons and 2) a semisolid pool that consists of macromolecular protons (9). Each pool has its own set of intrinsic longitudinal (T_1) and transverse (T_2) relaxation times. Magnetization exchange between the pools is modeled by a first-order rate constant (R).

Mathematically, the two-pool model is represented by the Bloch equations modified to include the effects of magnetization exchange (9). The time evolution of magnetization is determined by the solution to this system of differential equations. In continuous wave (CW) MT experiments, which apply a single, long ($>$5 s), constant-amplitude RF pulse, the magnetization can be determined by solving the modified Bloch equations with the assumption that the system is in the steady state (15). However, due to scan time limitations and specific absorption rate (SAR) concerns, in vivo MT experiments have to rely on multiple, short, shaped (e.g., Gaussian or Sinc) off-resonance pulses that are distributed throughout the imaging sequence. In this case, the steady-state solution is no longer valid. Since the duration of RF pulses is much shorter than the T_1 relaxation times of both pools and on the order of the liquid pool T_2 relaxation time, the behavior of magnetization can be determined only by solution of the modified Bloch equations in the time domain (15). The mathematical formalism is further complicated by the presence of shaped RF pulses with time-varying amplitudes.

To minimize the mathematical complexity associated with pulsed MT, several studies have proposed approximate methods for a simplified analysis of the experimental data. Sled and Pike (14) developed a signal equation that

[1]Department of Medical Biophysics, University of Toronto, Toronto, Canada.
[2]Imaging Research, Sunnybrook Health Sciences Centre, Toronto, Canada.
*Correspondence to: Greg J. Stanisz, Imaging Research, Sunnybrook Health, Sciences Centre, Rm. S672, 2075 Bayview Ave., Toronto, ON, Canada M4N 3M5. E-mail: stanisz@sri.ca

Received 31 May 2006; revised 19 February 2007; accepted 21 February 2007.
DOI 10.1002/mrm.21244
Published online in Wiley InterScience (www.interscience.wiley.com).

approximates the effect of an MT pulse on the liquid pool by an instantaneous saturation of longitudinal magnetization, and on the semisolid pool by a rectangular pulse of equal average power. Ramani et al. (16), citing the complexity of Sled and Pike's method, proposed an approach that extends the simplicity of CW MT analysis to pulsed experiments by computing the "continuous wave power equivalent" (CWPE) of the short MT pulses. Similarly, Yarnykh (13) proposed a technique that neglects the direct saturation of the liquid pool (direct effect) and approximates shaped RF pulses by equal-power rectangular pulses.

All of the above methods have contributed significantly to the current body of qMT research. However, potential differences in the MT parameters they obtain may complicate the comparison of reported results. The objective of the present study was therefore to determine the differences between MT parameters estimated using the techniques of Sled and Pike (14), Ramani et al. (16), and Yarnykh (13). To address this objective, the investigation was conducted in two parts. First, an MT modeling technique that makes minimal approximations, other than the use of a two-pool tissue representation, was developed and validated. Subsequently, this technique served as a standard against which to evaluate the other, more approximate models. Each model was used to fit experimental data obtained from samples of wild-type (WT) and *shiverer* mouse spinal cord, as well as simulated data generated using our minimal approximation modeling technique.

To our knowledge, this work constitutes the first systematic comparison of the pulsed MT models that are currently used in qMT investigations.

THEORY

In the presence of MT exchange, the time evolution of magnetization in the liquid (A) and semisolid (B) pools during an RF saturation pulse is given by the following system of equations (9):

$$\frac{\partial M_X^A}{\partial t} = -2\pi\Delta M_Y^A - \frac{M_X^A}{T_2^A} \quad [1a]$$

$$\frac{\partial M_Y^A}{\partial t} = 2\pi\Delta M_X^A - \omega_1 M_Z^A - \frac{M_Y^A}{T_2^A} \quad [1b]$$

$$\frac{\partial M_Z^A}{\partial t} = \omega_1 M_Y^A + R_A(M_0^A - M_Z^A) - RM_0^B M_Z^A + RM_0^A M_Z^B \quad [1c]$$

$$\frac{\partial M_Z^B}{\partial t} = R_B(M_0^B - M_Z^B) - (R_{RFB} + RM_0^A)M_Z^B + RM_0^B M_Z^A \quad [1d]$$

where x, y, and z denote the spatial components of a magnetization vector, Δ is the off-resonance frequency of the RF saturation pulse, and $\omega_1 = \gamma B_1$ is the angular precession frequency induced by the pulse. ${M_0}^A$ and ${M_0}^B$ are the equilibrium magnetizations of each pool, R_A and R_B are rate constants for the recovery of longitudinal magnetization ($=1/T_1$), and ${T_2}^A$ and ${T_2}^B$ are time constants describing the decay of transverse magnetization. The rate constants for the transfer of magnetization from the liquid to the semisolid pool and vice versa are $R{M_0}^B$ and $R{M_0}^A$, respectively. With the rate constants defined in this manner (i.e., explicitly in terms of the equilibrium magnetization of each pool), the variable R represents a fundamental MT exchange constant that is independent of the relative sizes of the liquid and semisolid pools (9). Typically, the magnetization of the liquid pool, ${M_0}^A$, is set to one. Therefore, ${M_0}^B$ represents the number of macromolecular protons, relative to ${M_0}^A$, that undergo MT exchange.

To describe the behavior of macromolecular protons, the Bloch equations for the semisolid pool are replaced by a single longitudinal component, where the saturation of magnetization is governed by the saturation rate, R_{RFB}:

$$R_{RFB} = \pi\omega_1^2 g_B(2\pi\Delta), \quad [2]$$

where g_B is the absorption lineshape, which is a function of the semisolid pool's transverse relaxation time constant, ${T_2}^B$. The integral of the lineshape function, $g_B(2\pi\Delta)$, over all frequencies, Δ, is equal to unity. For biological tissues, the semisolid lineshape is typically approximated by a super-Lorentzian (17):

$$g_B(2\pi\Delta) = \int_0^{\frac{\pi}{2}} d\theta \sin\theta \sqrt{\frac{2}{\pi}\frac{T_2^B}{|3\cos^2\theta - 1|}} \exp\left\{-2\left[\frac{2\pi\Delta T_2^B}{3\cos^2\theta - 1}\right]^2\right\} \quad [3]$$

Solving differential Eqs. [1a]–[1d] is relatively straightforward for CW MT experiments in which, due to steady-state conditions, all four time derivatives are equal to zero. By solving for M_Z^A, a relatively simple expression for signal intensity is obtained (9):

$$M_Z^A = \frac{R_B R M_0^B + R_{RFB} R_A + R_B R_A + R_A R}{\left(R_A\left[\frac{\omega_1^2 T_2^A}{1 + (2\pi\Delta T_2^A)^2}\right] + RM_0^B\right)(R_B + R_{RFB} + R) - RRM_0^B} \quad [4]$$

This solution does not apply to pulsed MT experiments, due to the short-duration RF pulses and time-varying pulse amplitudes. In general, the magnetization during a pulsed MT sequence is given by the following matrix differential equation (14):

$$\frac{dM(t)}{dt} = \Lambda(t)M(t) + \beta M_0, \quad [5]$$

where M is a 4D magnetization vector (M_X^A, M_Y^A, M_Z^A, M_Z^B) and the elements of vector M_0 are equal to the equilibrium value of each magnetization component. Λ and β are matrices corresponding to the coefficients of Eqs. [1a]–[1d]. When the matrix Λ is constant in time, as is the case with rectangular RF pulses or free precession, the following general analytical solution is obtained (18):

$$M(t) = e^{At}M(t = 0) + \Lambda^{-1}(e^{At} - I)\beta M_0 \quad [6]$$

However, when Λ is time-varying (due to amplitude-modulated RF pulses), no such general solution exists.

In an early investigation of the MT effects produced by shaped RF pulses, Graham and Henkelman (15) overcame this limitation by solving the modified Bloch equations numerically. In the numerical computation, the rate of saturation of the semisolid pool is calculated using Eq. [2], with the ω_1 term varying in time according to the RF pulse amplitude, B_1.

The technique used in the present study modeled the effects of amplitude-modulated RF pulses in a similar manner. However, rather than using a general numerical algorithm, the solution was calculated by dividing RF pulses into a series of short rectangular segments (50 μs in duration) whose envelope was described by the desired pulse shape. Equation [6] was then used to propagate the magnetization through each interval, with the endpoint values of one interval serving as initial conditions for the next one. The 50-μs duration was chosen since further decreases in the length of rectangular segments induced changes in the final solution of less than 1.5%. At offset frequencies above 800 Hz, the changes were less than 0.1%. By representing the shaped MT pulses in this manner, we were able to solve the modified Bloch equations using minimal approximations to describe the behavior of magnetization during and between RF saturation pulses. The only physical approximation was the assumption that tissues are accurately described by a two-pool model of MT exchange. For the remainder of this manuscript, we therefore refer to our method as the minimal approximation MT (MAMT) technique.

Sled and Pike (14), Ramani et al. (16), and Yarnykh (13) used more approximate approaches to handle the time-varying coefficients of Eqs. [1a]–[1d]. The specifics of these techniques are outlined in the sections that follow.

Sled and Pike's Approximation

The model proposed by Sled and Pike (14) is based on decomposing the pulse sequence into periods of free precession, constant-amplitude irradiation of the semisolid pool, and instantaneous saturation of the liquid pool. In all of these cases, the modified Bloch equations have constant coefficients and can be solved simply and analytically. For additional simplicity, only the longitudinal components of magnetization are modeled. Transverse components are assumed to disappear through relaxation and spoiling.

Two different approximations are used to describe the behavior of the liquid and semisolid pools. The effect of the shaped MT pulse on the liquid pool is modeled by an instantaneous fractional saturation of longitudinal magnetization. The saturation fraction, S_f, is obtained by solving Eqs. [1a]–[1c] numerically, taking into account the time-varying pulse amplitude but neglecting T_1 recovery and magnetization exchange (R_A, R, and M_0^B are set equal to zero). With the value of S_f calculated in advance, the effect of the shaped MT pulse can be modeled as instantaneous, such that

$$M_Z^{A+} = S_f M_Z^{A-}, \quad [7]$$

where the superscripts – and + refer to the magnetization immediately before and after the pulse, respectively. Before and after instantaneous saturation the liquid pool experiences free precession, with T_1 relaxation and exchange terms taken into account, which compensates for the elimination of these terms in the calculation of S_f. By describing liquid pool behavior in this manner, this model assumes that the rotation of liquid pool magnetization occurs independently of T_1 recovery and magnetization exchange processes.

The effect of the MT pulse on the semisolid pool is modeled by a rectangular pulse with equivalent average power. The duration of the rectangular pulse is equal to the full width at half maximum (FWHM) of the square of the original, shaped pulse. The condition of equivalent average power is fulfilled by ensuring that the time integrals of the square of the RF pulse envelopes,

$$\int_0^\tau \omega_1^2(t)\,dt \quad [8]$$

are equal (19). Such a description of the semisolid pool is based on the assumption that the saturation of macromolecular magnetization is not affected by the RF pulse shape.

With these approximations, the signal intensity is relatively simple to calculate, as analytical expressions exist for the longitudinal magnetization throughout each stage. To propagate the magnetization through the sequence, the endpoint values of one stage are simply used as initial conditions for the next one. Finally, a closed-form solution is obtained by imposing the condition that sufficient RF pulses have been applied to ensure that the pulsed steady state has been achieved (i.e., the magnetization behaves periodically with TR, the pulse repetition period).

Ramani et al.'s CWPE Approximation

Ramani et al. (16) approximated the pulsed MT sequence by means of a CW sequence with equivalent average power. Using this approximation, the expression for signal intensity is given by Eq. [4]; only the time-varying RF pulse amplitude, $\omega_1(t)$, is approximated by a constant CWPE saturation pulse amplitude, ω_{1CWPE}, given by:

$$\omega_{1CWPE} = \sqrt{\frac{\int_0^\tau \omega_1^2(t)\,dt}{TR}}, \quad [9]$$

where TR is the pulse repetition period of the original pulsed MT sequence, and the integral on the right-hand side is evaluated for the original shaped RF pulse. This guarantees that both the CW and pulsed MT sequence deposit equal average power per repetition period.

Yarnykh's Approximation

Yarnykh's (13) approach involves modeling the amplitude-modulated MT pulse by an *effective* rectangular

pulse of equal duration, τ. ω_{1eff}, the RF amplitude of the rectangular pulse is given by:

$$\omega_{leff} = \sqrt{\frac{1}{\tau}\int_0^{\tau} \omega_1^2(t)dt}, \quad [10]$$

which establishes that the effective pulse has equivalent average power. Yarnykh's (13) method also assumes that the offset frequency of the RF pulse is sufficiently large that it affects only the semisolid pool, and any direct saturation of the liquid pool can be neglected. In addition, much like Sled and Pike's approach, it does not model transverse components of magnetization (M_X^A and M_Y^A), assuming that any transverse magnetization disappears through the processes of T_2 relaxation and dephasing induced by spoiler gradients at the end of each RF pulse.

MATERIALS AND METHODS

MR Experiments

All NMR measurements were performed at 20°C and 1.5 Tesla on a 20-cm horizontal bore superconducting magnet (Nalorac, Martinez, CA, USA) controlled by a spectroscopy console (SMIS, Surrey, England). The experimental system did not include spatial encoding gradients. As such, all measurements represent an average across the entire sample.

The pulsed MT protocol consisted of a 7.5-s pulse train composed of 150 15-ms Gaussian pulses (167-Hz bandwidth) with a 50-ms TR. The pulse train was followed by a 90° on-resonance excitation pulse to measure the remaining longitudinal magnetization of the liquid pool. A total of 150 saturation pulses were sufficient to establish a pulsed steady state, whereby the time evolution of magnetization became periodic with the repetition period of the MT pulses.

To validate our MAMT technique, CW MT experiments were also performed. Unlike pulsed MT, CW data analysis is quick, simple, and well established. As such, fitted parameters obtained from CW MT data can serve as a gold standard for the comparison of pulsed MT parameter estimates. The CW MT sequence consisted of 7 s of constant amplitude off-resonance irradiation, followed by a 90° excitation pulse.

For both the CW and pulsed MT sequences a series of measurements with varying RF pulse amplitudes and frequency offsets were obtained. Specifically, 27 off-resonance irradiation frequencies, Δ, were logarithmically distributed from 14 Hz to 213 kHz. Data were collected at each of these offset frequencies for six different RF saturation pulse amplitudes ($\omega_1/2\pi$ = 0.17, 0.33, 0.67, 1.34, 2.67, and 5.34 kHz), resulting in a total of 192 data points. For the pulsed MT sequence, the on-resonance flip angles of the Gaussian saturation pulses that corresponded to each of these RF amplitudes were θ = 359°, 718°, 1436°, 2872°, 5745°, and 11490°.

Although all six of these RF amplitudes were included in the validation experiments, when the techniques of Sled and Pike (14), Ramani et al. (16) and Yarnykh (13) were used to fit pulsed MT data, only the two lowest RF amplitudes were included ($\omega_1/2\pi$ = 0.33, 0.17 kHz). By excluding the higher amplitudes, we achieved greater similarity to the in vivo MT protocols (which use low-power pulses due to SAR concerns) for which these approximate data analysis techniques were designed (7,16,20).

It has been noted by Henkelman et al. (9) that unique sets of all six two-pool model parameters (R_A, R_B, T_2^A, T_2^B, M_0^B, and R) cannot be obtained by fitting to steady-state MT data. Following the authors' approach, this was resolved by independently measuring R_{AOBS}, the *apparent* longitudinal relaxation rate for the liquid pool. R_{AOBS} was measured in an inversion-recovery (IR) sequence (21) with 15 inversion times logarithmically spaced from 1 to 32000 ms, 10 s between each acquisition and the next inversion pulse, and four averages.

The longitudinal relaxation rate, $R_{AOBS} = 1/T_{1OBS}$, measured in an IR sequence is, in general, not equal to the intrinsic longitudinal relaxation rate of water protons, R_A, due to MT exchange between the liquid and semisolid pools. However, the relationship between R_{AOBS} and R_A can be derived from the equation proposed by Henkelman et al. (9):

$$R_A = R_{AOBS} - \frac{RM_0^B(R_B - R_{AOBS})}{R_B - R_{AOBS} + R}. \quad [11]$$

Thus, independently measuring R_{AOBS} makes it unnecessary to fit for R_A, since it can be calculated using the remaining two-pool model parameters.

For completeness, T_2 relaxation data were acquired using a Carr-Purcell-Meiboom-Gill (CPMG) sequence (21,22) with TE/TR = 1/8000 ms, 3000 even echoes sampled, and eight averages.

Samples

Initial validation experiments were performed on a 0.1-mM $MnCl_2$ solution. Subsequent investigations were conducted on samples of WT and *shiverer* mouse spinal cord.

The *shiverer* mouse has an autosomal-recessive mutation characterized by an almost complete lack of central nervous system (CNS) myelin (23). This mutation is associated with the onset of tremors at about the 12th day of life, seizures at later times, and progressive deterioration ending in an early death (24). The lack of myelin is attributed to the absence of a functional copy of the gene that produces myelin basic protein (MBP), which accounts for 30–40% of the total protein in the myelin sheath (24).

Spinal cord samples were obtained from 10-week-old female mice that were killed by an overdose of pentobarbital sodium. Immediately after excision the samples were placed in nonprotonated, MR-compatible fluid (Flourinert; 3M, London, Canada) to prevent dehydration and reduce susceptibility artifacts. The samples were stored in a 4°C refrigerator prior to the MR experiments.

Fitting Procedure

MT parameters R, M_0^B, T_2^A, and T_2^B were estimated by nonlinear least-squares fitting of the model to the experimental data according to the method described in Ref. 25.

In contrast to Ref. 25, however, uncertainties in fitted parameters were expressed in terms of the 95% confidence interval (rather than 67%). In addition, when the upper and lower bounds of the confidence region for a particular parameter were determined, the remaining parameters were kept constant and not reoptimized.

Comparison of Other Models

Following validation, the MAMT technique was used to generate a pulsed MT dataset to be fitted using the models of Sled and Pike (14), Ramani et al. (16), and Yarnykh (13). Complete datasets consisted of 30 points (two RF amplitudes × 15 offset frequencies logarithmically distributed from 1.174 to 213 kHz). Two different pulsed MT sequences were simulated: one with 15-ms Gaussian pulses (θ = 359°, 718°) and one with 30-ms Gaussian pulses of equivalent average power (θ = 477°, 927°). Both MT sequences had a TR of 50 ms. These sequence parameters were chosen based on their similarity to those typically used in in vivo qMT protocols (7,13,14).

The MT parameters used in initial simulations were those obtained in Refs. 11 and 26 for WM, which include R_B = 1 s^{-1}, R_A = 1.4 s^{-1}, R = 21 s^{-1}, M_0^B = 13.3%, T_2^A = 31.1 ms, and T_2^B = 10.4 μs. Simulations mimicking the effects of the pathological process of demyelination were also conducted. It is widely accepted that MT effects in WM are primarily due to the exchange of magnetization between water and myelin lipids (23). Therefore, we simulated the process of demyelination by linearly decreasing the macromolecular proton fraction, M_0^B, from 13.3% (normal WM) to 2% (complete demyelination) (25). According to our previous work, the process of demyelination is accompanied by increases in water T_1 and T_2 relaxation times. As such, $T_1^A = 1/R_A$ and T_2^A were simultaneously increased up to 20% and 30% more than the normal values, respectively (25). The remaining MT parameters, such as the MT exchange rate, R, and the transverse relaxation time of the semisolid pool, T_{2B}, were kept constant since they do not vary significantly in WM pathologies (2,3,7). In total, data were generated for 11 different combinations of T_1^A, T_2^A, and M_0^B. Thus, fits were performed on a total of 22 simulated datasets (11 datasets/sequence × 2 sequences).

In all fits performed on simulated data, the true value of R_A (i.e., the one used to generate the data) was entered into the fitting procedure in advance. While it may seem impractical to provide the fit with the correct R_A, this is similar to most MT protocols, which supply data fits with estimates of the longitudinal relaxation rate obtained in independent IR experiments (12,20,27). By entering R_A into the fits, we are effectively simulating the case where an error-free estimate of R_{AOBS} is obtained.

Fitting procedures performed using the models of Sled and Pike (14) and Ramani et al. (16), included all 30 of the points within each dataset (which all had offset frequencies above 1 kHz). With Yarnykh's (13) approach, only data points with offset frequencies greater than 2.5 kHz were included. This is in agreement with the investigator's recommended cutoff frequency (in the range of 2–3 kHz), which was assigned because this technique ignores the direct saturation of the liquid pool.

In addition to these simulated data fits, which represent the hypothetical situation of an infinite signal-to-noise ratio (SNR), the three techniques were also used to fit experimental data from *shiverer* and WT mouse spinal cord samples.

RESULTS

The results of this investigation are presented and discussed in two parts. The first section describes the validation of the MAMT method, while the second describes the comparison of the techniques used by Sled and Pike (14), Ramani et al. (16), and Yarnykh (13). The results of the MT experiments are depicted as plots of normalized signal intensity (M_Z^A/M_0^A), vs. the offset frequency, Δ, with the x-axis in logarithmic scale. Often referred to as a z-spectrum (28), such a plot is commonly used in reporting MT findings.

Validation of the MAMT Technique

Initial experiments were performed on a 0.1-mM $MnCl_2$ solution. For this aqueous paramagnetic solution there is no macromolecular component, and the model therefore consists only of the liquid pool (R = 0, M_0^B = 0). This sample was chosen as a control since the results obtained do not represent MT, but only the direct effect of the off-resonance irradiation on the liquid pool. This initial experiment served to validate the mathematical formalism used to describe the RF saturation pulses.

Pulsed MT measurements of the 0.1-mM $MnCl_2$ solution are shown in Fig. 1 for a single RF amplitude (on-resonance flip angle, θ = 11490°). The solid line is the theoretical result, calculated directly using the measured re-

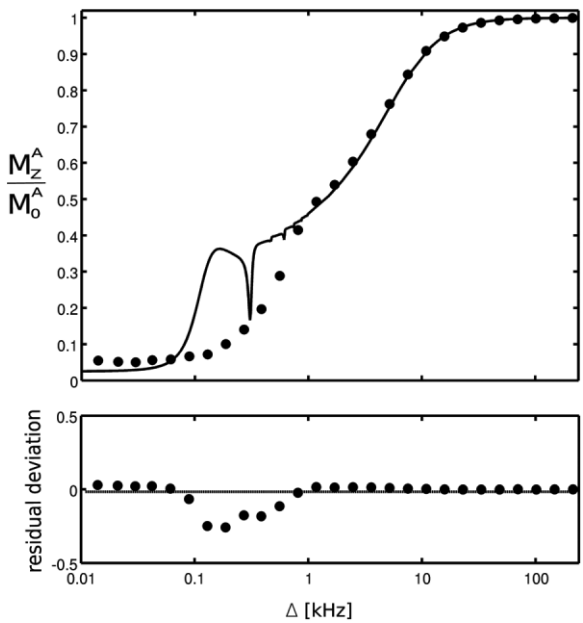

FIG. 1. Theory (solid line) vs. experiment (data points) for 0.1-mM $MnCl_2$. Pulse sequence parameters include 15-ms Gaussian pulses, maximum RF amplitude, $\omega_1/2\pi$ = 5.32 kHz, θ = 11490° and TR = 50 ms. Residuals are also shown.

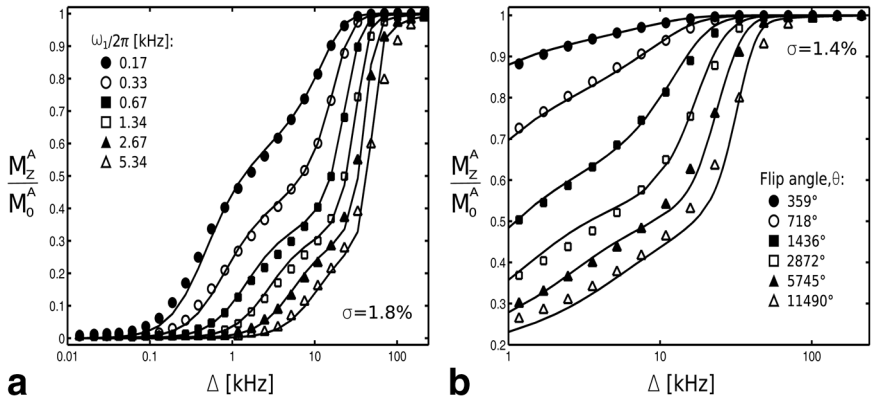

FIG. 2. (**a**) CW and (**b**) pulsed MT data for WT mouse spinal cord. In plot (a) the solid lines represent the fit of Eq. [4] to the data points, and in plot (b) the solid lines represent the fit of the MAMT model. For pulsed MT data the flip angle (θ) of the Gaussian pulses, rather than the maximum RF amplitude ($\omega_1/2\pi$), is indicated in the legend.

laxation times of the $MnCl_2$ sample (T_1 = 1.012 s; T_2 = 153 ms). At off-resonance frequencies above 1 kHz, the calculated curve and the experimental data agree very well. Below 1 kHz, the theoretical curve has sharp, oscillatory features that are not reflected experimentally. As a result of this disagreement, data points at offset frequencies below 1 kHz were excluded from fitting procedures performed on pulsed MT data.

For further validation of the proposed approach to pulsed MT modeling, the results of MT model fits performed on CW and pulsed MT data (obtained from samples of WT and *shiverer* mouse spinal cord) were compared. Figure 2 shows CW (a) and pulsed MT (b) data for the WT spinal cord sample. The six sets of curves on each plot correspond to six different RF saturation pulse amplitudes. On the CW plot (a) the solid lines represent the fit of Eq. [4] to the data, whereas on the pulsed MT plot (b) the solid lines represent the fit of the MAMT technique. Details of the fitting procedure are provided in Ref. 25. For pulsed MT, data below 1 kHz are not shown.

Agreement between the fitted curves and the experimental data is good, with average residual deviations per point, σ, of 1.8% for CW MT data and 1.4% for pulsed MT data. The MT parameters derived from fits to the experimental data are summarized in Table 1a. Specifically, the exchange rate, R, the semisolid pool fraction, M_0^B, and the transverse relaxation times of the liquid and semisolid pools, T_2^A and T_2^B, are shown. The longitudinal relaxation rate of the semisolid pool, R_B, is not presented since the experimental data were not sensitive to this parameter.

Uncertainties in the fitted parameters are expressed in terms of the 95% confidence interval. Since the confidence intervals were not always symmetric, the upper and lower limits are shown in parentheses. The longitudinal relaxation rates and transverse relaxation times obtained from independent experiments (R_{AOBS}, T_{2AOBS}) were (1.04 ± 0.1 s^{-1}, 106 ± 3 ms) and (1.29 ± 0.1 s^{-1}, 86 ± 4 ms) for the *shiverer* and WT samples, respectively.

Fitted parameters to pulsed and CW MT data agree within stated uncertainties. This serves to validate the MAMT technique. It is of note, however, that pulsed MT fits obtained much higher estimates of the exchange rate, R, with substantial uncertainty, as indicated by the width of the 95% confidence region. In addition, the exchange rate, R, and transverse relaxation time, T_2^A, varied significantly in response to fitting different subsets of the data. Table 1b shows the parameters estimated when only data points corresponding to the two lowest RF amplitudes ($\omega_1/2\pi$ = 0.33, 0.17 kHz) were included in CW and pulsed MT fits. RF amplitudes in this range are typical of in vivo MT protocols. In the CW MT fits, values of R and T_2^A were approximately 30% larger than those estimated using the entire data set. Values for the relative size of the semisolid pool, M_0^B, and transverse relaxation time, T_2^B, however, were independent of the choice of data points (less than 1% difference). With pulsed MT fits, changes in R and T_2^A occurred in the opposite direction: R decreased by about 80% and T_2^A decreased by 30%. Once again, changes in M_0^B and T_2^B were much less pronounced (<10%).

Table 1
Summary of Fitted MT Parameters

Sample	MT experiment	R (s^{-1})	M_0^B (%)	T_2^A (ms)	T_2^B (μs)	σ (%)
a: $\omega_1/2\pi$ = 5.34, 2.67, 1.34, 0.67, 0.33, 0.17 kHz						
Shiverer	CW	74 (58–97)	2.7 (2.3–3.2)	89 (60–134)	7.9 (6.9–9.0)	1.81
	Pulsed	132 (60–205)	2.5 (2.2–2.8)	74 (57–97)	9.1 (7.7–10.6)	1.39
Wild type	CW	70 (53–94)	4.3 (3.7–5.1)	55 (35–88)	8.4 (7.4–9.5)	1.81
	Pulsed	121 (69–198)	3.9 (3.4–4.4)	50 (37–71)	9.6 (8.2–11.2)	1.44
b: $\omega_1/2\pi$ = 0.33, 0.17 kHz						
Shiverer	CW	84 (62–120)	2.8 (2.6–3.0)	114 (83–158)	7.7 (6.0–9.9)	0.87
	Pulsed	32 (24–52)	2.6 (2.5–2.8)	50 (41–64)	8.4 (7.2–9.9)	0.21
Wild type	CW	82 (60–118)	4.4 (3.9–5.0)	74 (51–109)	8.5 (6.8–10.5)	0.89
	Pulsed	24 (19–32)	4.3 (4.0–4.6)	35 (29–46)	9.3 (8.3–10.1)	0.23

*Upper and lower limits of the 95% confidence interval are shown in parentheses.

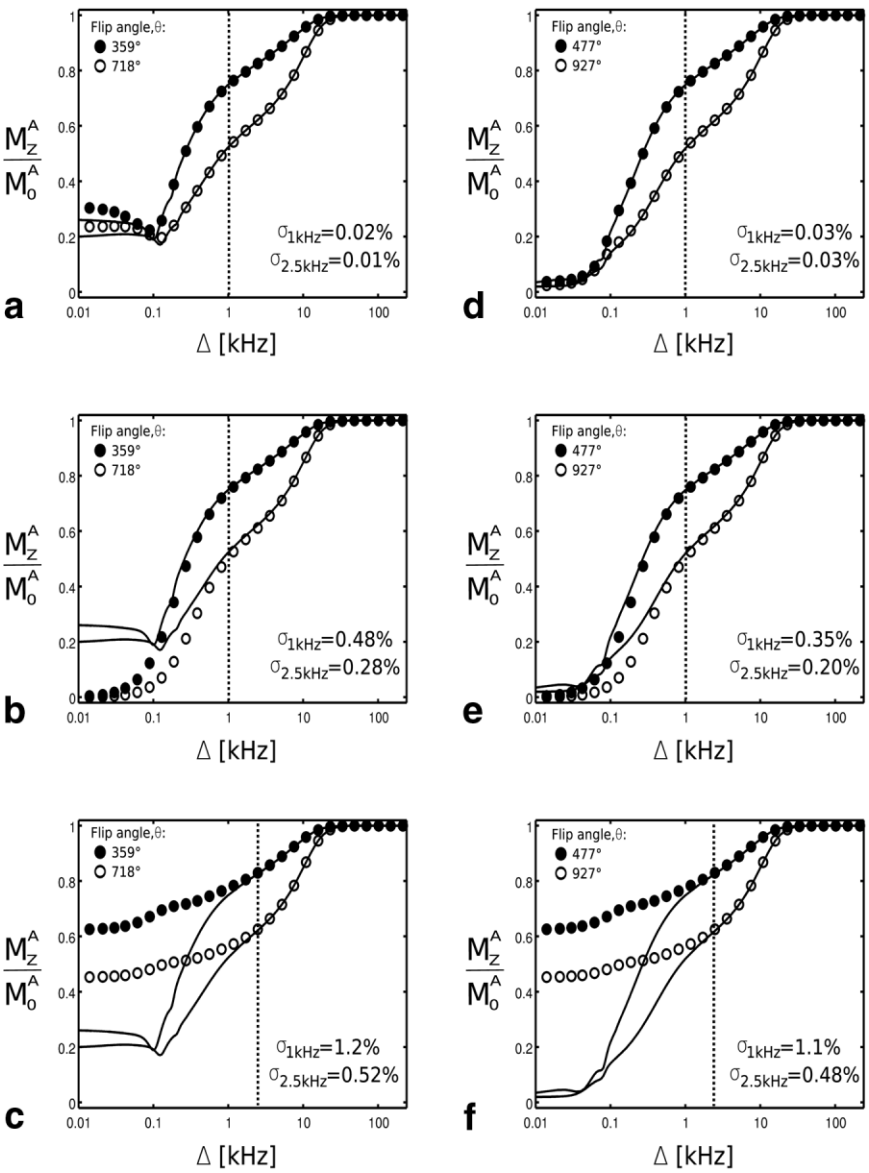

FIG. 3. Comparison of the pulsed MT models of (**a** and **d**) Sled and Pike (14), (**b** and **e**) Ramani et al. (16), and (**c** and **f**) Yarnykh (13) to the MAMT model (solid lines). Plots (a–c) are a simulation of sequence 1 (15-ms Gaussian pulses, 50-ms TR), and plots (d–f) are a simulation of sequence 2 (30-ms Gaussian pulses, 50-ms TR). Each plot contains two sets of curves that correspond to two different flip angles (sequence 1: θ = 359°, 718°; sequence 2: θ = 477°, 927°). Average residual deviations per point from our model are shown: σ_{1kHz} includes all points above 1 kHz in the calculation, and $\sigma_{2.5kHz}$ includes all points above 2.5 kHz. On each plot a dashed line indicates the cutoff off-resonance frequency below which all data points were rejected from fitting procedures.

Comparison of Other Models

Simulated *z*-spectra generated by the MAMT technique (solid lines), using the parameters obtained in Refs. 11 and 26 for healthy WM, are shown in Fig. 3. For comparison, *z*-spectra generated using the approximations of Ramani et al. (16), Sled and Pike (14), and Yarnykh (13) are also plotted. Simulated data for two different pulsed MT sequences are shown: one with 15-ms Gaussian pulses (sequence 1, plots a–c) and one with 30-ms Gaussian pulses (sequence 2, plots d–f). Solid lines are the MAMT predictions, while the data points are the predictions of the other, more approximate models. Each plot contains two sets of curves that correspond to two different RF saturation pulse amplitudes ($\omega_1/2\pi$ = 0.33, 0.17 kHz).

A dashed line on each plot indicates a cutoff off-resonance frequency. Points below this cutoff were excluded from fitting procedures performed on both simulated and experimental pulsed MT data. As indicated, data fits performed using the models of Sled and Pike (14) and Ramani et al. (16). excluded any points below 1 kHz. This 1-kHz cutoff was chosen due to the findings of the previous section (see Fig. 1), since it would be inappropriate to evaluate these techniques in a region where even the MAMT model did not agree with the data. Since it did not account for the direct effect, Yarnykh's (13) model had an even higher cutoff of 2.5 kHz.

The average deviation from the MAMT model per point (σ) is shown in the bottom right corner of the plots. For completeness, two values of σ are indicated: σ_{1kHz} includes all points with offset frequencies above 1 kHz in the calculation, and $\sigma_{2.5}$ kHz includes all points above 2.5 kHz.

Of the three techniques, Sled and Pike's (14) was the most similar to the MAMT model. The other two models agreed with it poorly at low offset frequencies, but gradually improved with increasing offset frequency, Δ. Below approximately 1 kHz, Ramani et al.'s (16) CWPE approximation consistently underestimated the MAMT model. In

Table 2
Summary of Fitted MT Parameters

	R (s^{-1})	M_0^B (%)	T_2^A (ms)	T_2^B (μs)	σ (%)
a: Wild type spinal cord					
Sled and Pike (14)	25 (19–60)	4.3 (4.0–4.5)	36 (29–47)	9.3 (7.9–10.9)	0.23
Ramani et al. (16) (CWPE)	20 (17–25)	4.3 (4.1–4.6)	40 (31–54)	9.4 (8.0–11.1)	0.25
Yarnykh (13) (2.5 kHz cutoff)	54 (28–184)	4.0 (3.7–4.4)	n/a	9.3 (7.5–11.5)	0.30
Yarnykh (13) (1 kHz cutoff)	84 (30–554)	4.0 (3.4–4.7)	n/a	10.9 (7.6–16.1)	0.67
MAMT	24 (19–32)	4.3 (4.0–4.6)	35 (29–46)	9.3 (8.3–10.1)	0.23
b: *Shiverer* spinal cord					
Sled and Pike (14)	34 (24–60)	2.6 (2.4–2.8)	52 (42–67)	8.4 (7.2–9.9)	0.21
Ramani et al. (16) (CWPE)	26 (20–34)	2.6 (2.5–2.8)	57 (46–75)	8.5 (7.2–10.1)	0.22
Yarnykh (13) (2.5 kHz cutoff)	176 (45–500)	2.4 (2.2–2.6)	n/a	8.4 (7.0–10.5)	0.27
Yarnykh (13) (1 kHz cutoff)	1070 (71–5000)	2.3 (1.9–2.7)	n/a	9.8 (7.0–13.9)	0.73
MAMT	32 (24–52)	2.6 (2.5–2.8)	50 (41–64)	8.4 (7.2–9.9)	0.21

n/a = parameter not estimated.

contrast, Yarnykh's (13) approach consistently and significantly overestimated it.

Parameter estimates obtained from fitting the simulated MAMT datasets using the three techniques are plotted in Fig. 4. The true parameter values (i.e., the ones used to generate the data) are indicated by dashed lines superimposed on each plot. While there are differences in estimates of R, T_2^A, and T_2^B, estimates of M_0^B were remarkably similar among the three techniques, never deviating by more than 6% from the correct value. In general, Sled and Pike's (14) model produced the most accurate parameter estimates. Ramani et al.'s CWPE approximation consistently underestimated the MT exchange rate, R, (by roughly 15%) and overestimated the transverse relaxation time of the liquid pool, T_2^A (by about 12%). Yarnykh's (13) approach consistently overestimated R and T_2^B, with the amount of error decreasing exponentially with increasing values of the semisolid pool fraction, M_0^B.

Fitted MT parameters for the experimental spinal cord data are summarized in Table 2. Results are shown for each of the three techniques as well as the MAMT model. For completeness, parameters obtained by Yarnykh's (13) model when all points above 1 kHz were included in the fit are also shown.

As with the simulated data, estimates of M_0^B, the macromolecular proton fraction, were very similar for all four models. Fitted values for the semisolid pool transverse relaxation time, T_2^B, were also very close. In general, parameters estimated by Sled and Pike's (14) model were closest to those obtained using the MAMT technique. The CWPE approximation resulted in lower estimates of the MT exchange constant, R, and longer values of the liquid pool transverse relaxation time, T_2^A. With all data points above 1 kHz included, Yarnykh's (13) model did not perform as well. The quality of the fit was reduced (higher σ) and the MT exchange rate, R, was significantly overesti mated (with substantial uncertainty), particularly in the *shiverer* mouse. The transverse relaxation time of the semisolid pool, T_2^B, was also overestimated. However, performance improved with the 2.5-kHz cutoff.

DISCUSSION

qMT techniques provide specific information about tissue microstructure. qMT parameters such as the semisolid pool fraction, M_0^B, the MT exchange rate, R, and the semisolid pool transverse relaxation time, T_2^B, are independent of experimental conditions such as the MT saturation scheme (9) or the external magnetic field (9,29). Therefore, they provide an objective measure of tissue pathology and are sensitive to changes in tissue microstructure. In particular, the semisolid pool fraction, M_0^B, is an indirect measure of myelin content in WM (3), whereas the MT exchange rate, R, and the semisolid pool transverse relaxation time, T_2^B, may reveal changes in the macromolecular composition of tissue. It is therefore important to determine MT parameters accurately and, if possible, without bias. In addition, data analysis should be computationally efficient, so that estimation of the MT parameters at every voxel in an image or region of interest (ROI) is feasible (14). To meet the latter requirement, many approaches use approximations that simplify and speed up the solution of the modified Bloch equations. It is, however, important to evaluate whether mathematical simplifications, which are used to reduce the computational time, result in unphysical estimates of the MT parameters. This was the rationale for this investigation.

Validation of the MAMT Model

Results obtained from validating the MAMT model highlight several issues that require consideration. First, the discrepancy between the model and the $MnCl_2$ data at low off-resonance frequencies ($\Delta < 1$ kHz) must be addressed. This disagreement was observed previously (25) and can be explained as follows:

During an MT saturation pulse, liquid pool magnetization precesses in a cone about the rotating frame effective magnetic field, B_{eff}. This leads to transient oscillations of both transverse and longitudinal magnetization, known as Rabi oscillations, which decay as the cone of precession tightens around B_{eff} (30). If the MT saturation pulses are not long enough for the Rabi oscillations to decay completely ($\sim 5T_{2\rho}$), oscillations will be observed in the z-spectrum. Considering that the saturation pulses used in this investigation were only 15 ms long, it is surprising that no oscillations appear in the experimental data. Some oscillations were, however, observed in an experiment with a smaller $MnCl_2$ sample (0.1 mL, instead of 5 mL). This suggests that the discrepancy in Fig. 1 may be due to

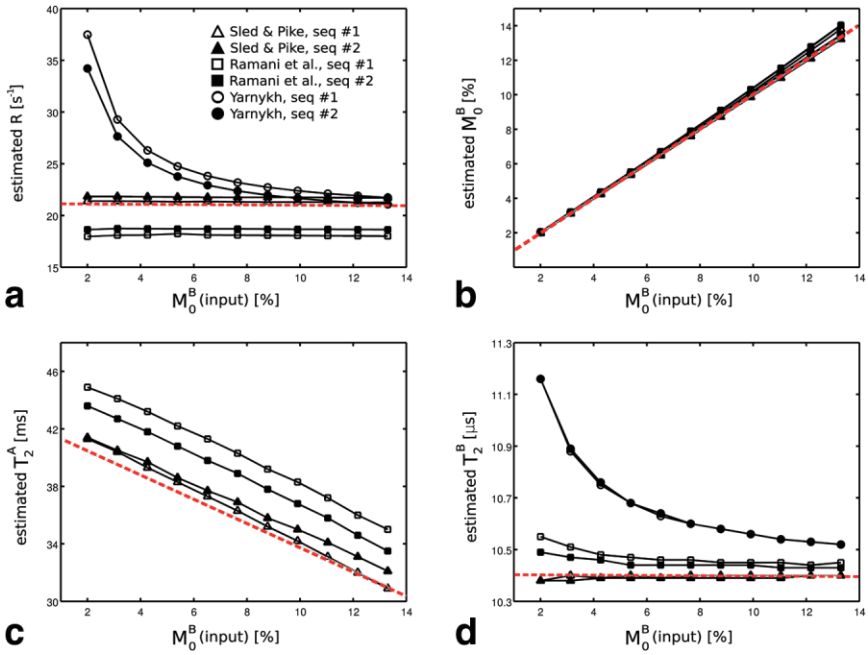

FIG. 4. Estimates of (**a**) R, (**b**) $M_0{}^B$, (**c**) $T_2{}^A$, and (**d**) $T_2{}^B$ obtained from fitting simulated pulsed MT data, which were generated using the MAMT model. The x-axis shows the values of $M_0{}^B$ that were used to generate each dataset. A dashed line on each plot indicates the correct parameter values. The legend is in the upper left plot (a). Plot C does not show $T_2{}^A$ estimates obtained using Yarnykh's (13) approach, since it did not estimate this parameter.

inhomogeneities in the B_1 and B_0 magnetic fields, which have a smoothing effect. Such smoothing is a particular problem in sequences like the one used in the present study and Ref. 25. Since these sequences lack spatial encoding, the signal obtained is integrated over the entire sample and therefore reflects an average over a range of experimental conditions. Similar difficulties were, however, encountered by Sled and Pike (14), whose protocol, unlike ours, involved both spatial encoding and B_1 field mapping. Surprisingly, though, the problem was reversed, in that oscillations were observed experimentally at low off-resonance frequencies (<800 Hz) but were not predicted by the model used.

In any event, these findings indicate that in pulsed MT experiments it is difficult to model the behavior of magnetization at low off-resonance frequencies. In the presence of field inhomogeneities, accurate modeling at low offset frequencies requires a complete characterization of the B_1 and B_0 field distributions throughout the sample. For the sake of simplicity, however, it is much more desirable to apply a 1-kHz cutoff to fitting procedures. This should not pose a problem since signal changes at these low offset frequencies occur largely due to direct saturation of the liquid pool and are likely independent of the sample's MT properties (14).

Additional systematic differences between the model and the data were observed at large saturation pulse amplitudes and large offset frequencies in both CW and pulsed MT fits. These differences were also observed previously (17,25) and are likely a result of using a two-pool tissue approximation. It has been suggested that the two-pool model may not be an appropriate description for MT in neural tissues, as T_2 relaxation studies indicate that transverse magnetization within WM does not decay monoexponentially (31). In particular, WM is known to exhibit two T_2 decay time constants: one associated with water in the intra-/extracellular space (70 ms $< T_2 <$ 200 ms) and one attributed to water within the myelin sheaths (10 ms $< T_2 <$ 50 ms) (32). Since there are two separable T_2 components within WM, a number of investigators have proposed a four-pool model for MT in which two pools of water protons, each with their own set of T_1 and T_2 relaxation times, exchange with one another and with their respective macromolecular pools (25,31). The complete system consists of a total of 15 parameters (compared to the six parameters of the two-pool system).

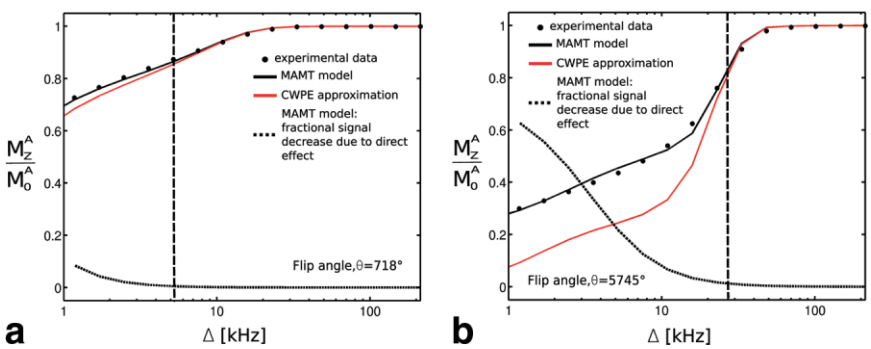

FIG. 5. Comparison of the CWPE and MAMT models to experimental data with MT saturation pulse flip angles of (**a**) 718° and (**b**) 5745°.

Although the four-pool model has demonstrated improved agreement with experimental data (25), using this system involves nearly tripling the number of fitted parameters. In order to accurately constrain these additional parameters, many more data points would have to be collected. For a four-pool model fit to CW MT data, Ref. 25 reported an average residual deviation per point, σ, of 1.2%, compared to the 1.8% deviation observed in this study. This small difference does not provide sufficient information with which to effectively determine nine more MT parameters. As such, parameter couplings and physically unreasonable parameter estimates are likely to result.

This is not to say, however, that a complete characterization of the four-pool model does not provide useful information. Nevertheless, the data obtained from typical MT experiments, which measure longitudinal magnetization following several seconds of off-resonance irradiation, are not sufficient to perform this task. A much wider range of experimental data is required, which can be obtained by collecting MT data in the transient state (using shorter saturation pulses) and combining MT with CPMG (25). On the time scale of typical MT experiments, complete mixing occurs between the various liquid T_2 components. In this context, the T_2 components may be viewed to merge, forming a single pool with a T_2 relaxation time equal to the reciprocal of the mean transverse relaxation rate (i.e., $\langle R_2 \rangle^{-1}$). Therefore, models like the ones discussed in the present study, which account for only a single liquid pool with a single T_2 value, are able to fit typical (steady-state) MT data reasonably well.

Fitted parameters estimated using the MAMT model agreed, within stated uncertainties, with parameters obtained from the "gold standard" CW MT data. However, no estimate of the longitudinal relaxation rate of the semisolid pool, R_B, was obtained, since the quality of the fit was not sensitive to this parameter. The inability to constrain R_B is consistently noted throughout the MT literature (2,3,7,9) and is a result of model insensitivity to this parameter, given the limited extent of experimental data.

It was also observed that relative to CW MT, pulsed MT data fits obtained much higher estimates of the exchange rate R, with substantial uncertainty. To determine whether this was a result of excluding data points below 1 kHz from fits to pulsed MT data, CW MT fits were repeated with the same cutoff frequency. This did not improve the agreement.

Of additional concern is the variability in the exchange rate, R, and transverse relaxation time, $T_2{}^A$, that occurred when different subsets of the experimental data were included in the fits. A number of factors may contribute to this inconsistency. The experimental data are less sensitive to R and $T_2{}^A$, and these parameters may be affected by systematic errors between the model and the data, which can vary depending on the choice of off-resonance frequency and RF power. Interestingly, however, a comparison of parameters in the *shiverer* and WT samples shows that the general trend in R and $T_2{}^A$ is consistent regardless of the experiment (pulsed or CW) or the data points included (i.e., no significant change is observed in R, and $T_2{}^A$ is increased in the *shiverer* sample). Thus, values of R and $T_2{}^A$ may be comparable across different samples or ROIs, provided the data are collected with identical protocols.

Further comparison of the two samples reveals that estimates of the fractional size of the semisolid pool, $M_0{}^B$ are consistently about 35% larger in the WT sample. This supports the hypothesis that this parameter is correlated with myelin content (3). In addition, longer transverse ($T_2{}^A$, $T_2{}^A{}_{\mathrm{OBS}}$) and longitudinal relaxation times ($R_{AOBS}{}^{-1}$) were observed in the *shiverer* spinal cord. This observation is consistent with the principle that relaxation is enhanced by the immobilization of tissue water on the surface of macromolecules (33).

Comparison of Other Models

The comparison of the techniques used by Sled and Pike (14), Ramani et al. (16), and Yarnykh (13) revealed that the approximations used in pulsed MT modeling are generally quite robust. Within the range of offset frequencies included in the data fits, all three of these approximate models were roughly consistent with MAMT predictions (see Fig. 3). However, with Ramani et al's (16) CWPE approximation and Yarnykh's (13) approach, which both have more restrictive approximations, some systematic deviations were visible.

In particular, the mean residual deviation per point between the CWPE approximation and the MAMT model was decreased for the sequence with the longer MT pulse (and shorter interpulse spacing). This is not surprising, since a sequence with a larger duty cycle is more similar to a CW saturation scheme. Below approximately 2 kHz, Yarnykh's (13) model consistently overestimated MAMT predictions. This is obviously a result of neglecting the direct effect.

In spite of these differences, results suggest that the semisolid pool fraction, $M_0{}^B$, and transverse relaxation time, $T_2{}^B$, can be evaluated with reasonable accuracy regardless of the model used. In contrast, estimates of the exchange rate, R, and transverse relaxation time, $T_2{}^A$, were model dependent. It is worth noting, however, that, the differences in R and $T_2{}^A$ estimates between the WT and *shiverer* samples were generally consistent (with all techniques other than Yarnykh's (13)). Even so, given the dependence on the experimental conditions and the difficulty in constraining these parameters with even the MAMT model, any interpretation based on R and $T_2{}^A$ should be made with caution.

The reduced accuracy of parameters estimated by Yarnykh's (13) technique when all data points above 1 kHz were included in the fit (see Table 2a and b) highlights the importance of an appropriately chosen cutoff offset frequency. It is therefore necessary to consider whether a change in the experimental conditions (e.g., RF power and field strength) could shift the location of the cutoff. In the case of Yarnykh's (13) approach, the 2.5-kHz cutoff was chosen because it was sufficiently far from resonance to ensure that the direct effect was, in fact, negligible. If the direct effect were to persist at higher offset frequencies, the cutoff would have to be increased. This is similarly true of Ramani et al's (16) CWPE approximation, although it may not be as obvious, since this technique does take direct saturation into account.

The limitations of the CWPE model are illustrated in Fig. 5. Figure 5a shows the experimental pulsed MT data from the WT mouse spinal cord sample, along with theoretical *z*-spectra generated by the MAMT and CWPE techniques. Also plotted is the fractional decrease in longitudinal magnetization (M_Z^A) that resulted only from direct saturation of the liquid pool (i.e., direct effect). Only points with offset frequencies above 1 kHz are included in the figure. Since the component of signal loss that occurs solely due to direct saturation cannot be determined experimentally, the direct effect curve was simulated using the MAMT model. This model has been demonstrated to predict experimental data reliably at offset frequencies greater than 1 kHz. Therefore, it stands to reason that the direct effect predictions shown in Fig. 5 are accurate.

In Fig. 5a the MAMT model and the experimental data agree throughout the entire range of offset frequencies shown ($\Delta > 1$ kHz). However, the CWPE approximation does not converge with the data until $\Delta \approx 5$ kHz (dotted line). As indicated by the plot of the direct effect, within this range of offset frequencies ($\Delta \geq 5$ kHz), direct saturation is responsible for less than 1% of the reduction in M_Z^A.

Figure 5b shows a similar set of *z*-spectra, but with a flip angle, θ, of 5745°. With the larger flip angle the direct effect is not reduced to 1% until $\Delta \approx 12$ kHz. As before, the MAMT model and the experimental data agree. However, the region of agreement between the CWPE model and the data has shifted, along with the direct effect, to $\Delta \geq 12$ kHz (dotted line). As such, in the event that a larger flip angle is chosen for the saturation pulse, unlike the MAMT technique, both Yarnykh's (13) model and the CWPE approximation will require an increased cutoff frequency. Variations in relaxation properties (increased T_1 and/or decreased T_2), such as those induced by changes in field strength or the use of contrast agents, could also cause the direct effect to persist at higher offset frequencies. Therefore, in these cases a reassessment of the cutoff may also be necessary.

The behavior of the CWPE approximation may be explained by its adequacy in describing the behavior of the semisolid pool, but inability to characterize the liquid pool. As the direct effect diminishes, changes in the MRI signal are no longer a result of saturating water protons. Thus, signal intensity is less dependent on the poorly characterized behavior of liquid pool magnetization. In the absence of the direct effect, signal changes are solely due to the transfer of magnetization to the semisolid pool, whose behavior is accurately characterized by the CWPE model. Indeed, the semisolid pool, with its extremely short T_2 relaxation time, may be easier to model since any transverse magnetization produced by an RF pulse is negligible and the concept of a flip angle does not apply (15). Under these circumstances, the only effect of RF irradiation is a depletion of the longitudinal magnetization.

Although the MAMT model and Sled and Pike's approach are more effective at characterizing liquid pool behavior, a 1-kHz cutoff was still assigned due to theoretical oscillations, which were not reflected experimentally. A similar analysis of the effects of experimental conditions and relaxation properties on the position of this cutoff is therefore necessary. This requires a more detailed explanation of the phenomenon of *z*-spectrum oscillations.

The fact that the oscillations in Fig. 1 subside by 1 kHz is a result of the Gaussian-shaped MT saturation pulses. During these amplitude-modulated pulses the rotating frame effective magnetic field, B_{eff}, is not stationary (as the RF amplitude increases, B_{eff} tips towards the transverse plane; when it decreases, B_{eff} tips back to the *z*-axis). If this movement of B_{eff} occurs slowly enough, then, rather than precessing around it, the magnetization becomes "spin locked" and simply follows the direction of the effective magnetic field (34). Without the precession there are no Rabi oscillations, and hence there are no oscillations in the *z*-spectrum. For the Gaussian pulses used in this investigation, the conditions for spin locking are fulfilled at an offset frequency of 1 kHz. With this value of Δ, the *z*-component of the effective magnetic field is large enough that the discontinuity in the direction of B_{eff}, which occurs at the start of each RF pulse, is minimal. Thus, the movement of B_{eff} is slow enough that the magnetization becomes spin locked and is restored along the *z*-axis at the end of the pulse.

The effect of experimental parameters and relaxation properties on the cutoff frequency can be determined according to the explanation above. The fulfillment of the conditions for spin locking is not affected by T_1 and T_2 relaxation times. Therefore, variations in relaxation properties will not shift the cutoff frequency. Increases in RF power could have an effect, but, as demonstrated by Fig. 1, even with a flip angle of 11490°, the 1 kHz cutoff is sufficient. A more noticeable effect would be observed with a change in the shape of the MT saturation pulses. In experiments conducted with rectangular pulses, for instance, the discontinuity in B_{eff} at the start of the pulse was never small enough to allow spin locking, and the oscillations were observed to persist well past 1 kHz. This problem can, however, be avoided with the careful selection of MT saturation pulses.

In summary, the cutoff frequencies assigned in this investigation were suitable for the RF saturation pulse amplitudes typically used in clinical MT protocols, and the range of MT parameters typically encountered in both normal and diseased WM. However, as demonstrated by the discussion above, under different experimental conditions a reevaluation of the assigned cutoffs may be necessary, particularly with the more approximate techniques of Ramani et al. (16) and Yarnykh (13).

It should also be noted that pulsed MT models other than the ones investigated here do exist, but were not selected for inclusion in this study. In particular, in a more recent publication, Yarnykh and Yuan (20) proposed a variant of the previous Yarnykh (13) model that contains an additional term to account for the direct effect. The model is still, however, only correct for relatively high offset frequencies, since the added term does not account for the rotation of the liquid pool magnetization that occurs closer to resonance. Therefore, we believe that a full investigation of this slightly modified technique was not warranted in this study. In addition, Helms and Hagberg (35) and Gochberg and Gore (36) proposed models for the analysis of pulsed MT data that were not considered here because they are not directly applicable to the *z*-spectroscopy experiments used in this investigation.

CONCLUSIONS

The present study shows that with the proper precautions, the semisolid pool fraction, M_0^B, and transverse relaxation time, T_2^B, can be accurately estimated even with a high degree of approximation. Reported values of these parameters may now be compared directly, regardless of the model that was used to obtain them. The stability and reliability of M_0^B estimates is particularly encouraging, since it is an MT parameter that has a true biological meaning (i.e., the relative number of hydrogen protons that are bound to macromolecules) and may directly reflect tissue composition (37). Furthermore, M_0^B has been observed to change dramatically in WM pathologies, particularly demyelination.

Some more caution may be required for the interpretation of the MT exchange rate, R, and the liquid pool transverse relaxation time, T_2^A, since these parameters are poorly constrained by the data and depend on the experimental protocol, as well as the model used to estimate them. The exchange rate, R, however, has demonstrated limited sensitivity to WM pathology (2,3,7). Although the transverse relaxation time, T_2^A, does change with disease, transverse relaxation properties of liquid pool magnetization can always be investigated with conventional spin-echo experiments.

In this study we have focused on the use of pulsed MT models for the evaluation of WM disease. There is, however, increasing interest in using MT to evaluate pathologies in other tissues (e.g., cartilage (38) and cancer (39)). Since the MR properties and MT phenomena differ among such tissues, the validity of the approaches studied and the implications of the results would have to be reevaluated.

REFERENCES

1. Wolff SD, Balaban RS. Magnetization transfer contrast (MTC) and tissue water proton relaxation in-vivo. Magn Reson Med 1989;10:135–144.
2. Stanisz GJ, Webb S, Munro CA, Pun T, Midha R. MR properties of excised neural tissue following experimentally induced inflammation. Magn Reson Med 2004;51:473–479.
3. Odrobina EE, Lam TYJ, Pun T, Midha R, Stanisz GJ. MR properties of excised neural tissue following experimentally induced clemyelination. NMR Biomed 2005;18:277–284.
4. van Waesberghe JHTM, Kamphorst W, De Groot CJA, van Walderveen MAA, Castelijns JA, Ravid R, Nijeholt GJLA, van der Valk P, Polman CH, Thompson AJ, Barkhof F. Axonal loss in multiple sclerosis lesions: magnetic resonance imaging insights into substrates of disability. Ann Neurol 1999;46:747–754.
5. Dousset V, Grossman RI, Ramer KN, Schnall MD, Young LH, Gonzalezscarano F, Lavi E, Cohen JA. Experimental allergic encephalomyelitis and multiple-sclerosis-lesion characterization with magnetization transfer imaging. Radiology 1992;182:483–491.
6. Schmierer K, Scaravilli F, Altmann DR, Barker GJ, Miller DH. Magnetization transfer ratio and myelin in postmortem multiple sclerosis brain. Ann Neurol 2004;56:407–415.
7. Sled JG, Pike GB. Quantitative imaging of magnetization transfer exchange and relaxation properties in vivo using MRI. Magn Reson Med 2001;46:923–931.
8. Filippi M, Rocca MA. Magnetization transfer magnetic resonance imaging in the assessment of neurological diseases. J Neuroimaging 2004; 14:303–313.
9. Henkelman RM, Huang XM, Xiang QS, Stanisz GJ, Swanson SD, Bronskill MJ. Quantitative interpretation of magnetization-transfer. Magn Reson Med 1993;29:759–766.
10. Pike GB. Pulsed magnetization transfer contrast in gradient echo imaging: a two-pool analytic description of signal response. Magn Reson Med 1996;36:95–103.
11. Morrison C, Henkelman RM. A model for magnetization-transfer in tissues. Magn Reson Med 1995;33:475–482.
12. Tozer D, Ramani A, Barker GJ, Davies GR, Miller DH, Tofts PS. Quantitative magnetization transfer mapping of bound protons in multiple sclerosis. Magn Reson Med 2003;50:83–91.
13. Yarnykh VL. Pulsed Z-spectroscopic imaging of cross-relaxation parameters in tissues for human MRI: theory and clinical applications. Magn Reson Med 2002;47:929–939.
14. Sled JG, Pike GB. Quantitative interpretation of magnetization transfer in spoiled gradient echo MRI sequences. J Magn Reson 2000;145:24–36.
15. Graham SJ, Henkelman RM. Understanding pulsed magnetization transfer. J Magn Reson Imaging 1997;7:903–912.
16. Ramani A, Dalton C, Miller DH, Tofts PS, Barker GJ. Precise estimate of fundamental in-vivo MT parameters in human brain in clinically feasible times. Magn Reson Imaging 2002;20:721–731.
17. Morrison C, Stanisz G, Henkelman RM. Modeling magnetization-transfer for biological-like systems using a semisolid pool with a super-Lorentzian lineshape and dipolar reservoir. J Magn Reson Ser B 1995; 108:103–113.
18. Martin, RH. Elementary differential equations with boundary value problems. New York: McGraw Hill Book Co.; 1984.
19. Magnetic resonance imaging: physical principles and sequence design. New York: Wiley-Liss; 1999.
20. Yarnykh VL, Yuan C. Cross-relaxation imaging reveals detailed anatomy of white matter fiber tracts in the human brain. Neuroimage 2004;23:409–424.
21. Carr HY, Purcell EM. Effects of diffusion on free precession in nuclear magnetic resonance experiments. Phys Rev 1954;94:630–638.
22. Meiboom S, Gill D. Modified spin-echo method for measuring nuclear relaxation times. Rev Sci Instrum 1958;29:688–691.
23. Barkovich AJ. Concepts of myelin and myelination in neuroradiology. Am J Neuroradiol 2000;21:1099–1109.
24. Molineaux SM, Engh H, Deferra F, Hudson L, Lazzarini RA. Recombination within the myelin basic-protein gene created the dysmyelinating shiverer mouse mutation. Proc Natl Acad Sci USA 1986;83:7542–7546.
25. Stanisz GJ, Kecojevic A, Bronskill MJ, Henkelman RM. Characterizing white matter with magnetization transfer and T_2. Magn Reson Med 1999;42:1128–1136.
26. Harrison R, Bronskill MJ, Henkelman RM. Magnetization-transfer and T_2 relaxation components in tissue. Magn Reson Med 1995;33:490–496.
27. Sled JG, Levesque I, Santos AC, Francis SJ, Narayanan S, Brass SD, Arnold DL, Pike GB. Regional variations in normal brain shown by quantitative magnetization transfer imaging. Magn Reson Med 2004;51:299–303.
28. Grad J, Mendelson D, Hyder F, Bryant RG. Applications of nuclear magnetic cross-relaxation spectroscopy to tissues. Magn Reson Med 1991;17:452–459.
29. Stanisz GJ, Odrobina EE, Pun J, Escaravage M, Graham SJ, Bronskill MJ, Henkelman RM. T_1, T_2 relaxation and magnetization transfer in tissue at 3T. Magn Reson Med 2005;54:507–512.
30. Henkelman RM, Stanisz GJ, Graham SJ. Magnetization transfer in MRI: a review. NMR Biomed 2001;14:57–64.
31. Bjarnason TA, Vavasour IM, Chia CLL, MacKay AL. Characterization of the NMR behavior of white matter in bovine brain. Magn Reson Med 2005;54:1072–1081.
32. Mackay A, Whittall K, Adler J, Li D, Paty D, Graeb D. In-vivo visualization of myelin water in brain by magnetic-resonance. Magn Reson Med 1994;31:673–677.
33. Kucharczyk W, Macdonald PM, Stanisz GJ, Henkelman RM. Relaxivity and magnetization transfer of white matter lipids in MR imaging—importance of cerebrosides and pH. Radiology 1994;192:521–529.
34. Moran PR, Hamilton CA. Near-resonance spin-lock contrast. Magn Reson Imaging 1995;13:837–46.
35. Helms G, Hagberg GE. Pulsed saturation of the standard two-pool model for magnetization transfer. Part I: The steady state. Concepts Magn Reson 2004;21A:37–49.
36. Gochberg DF, Gore JC. Quantitative imaging of magnetization transfer using an inversion recovery sequence. Magn Reson Med 2003;49:501–505.
37. Ropele S, Seifert T, Enzinger C, Fazekas F. Method for quantitative imaging of the macromolecular ^{1}H fraction in tissues. Magn Reson Med 2003;49:864–871.
38. Henkelman RM, Stanisz GJ, Menezes N, Burstein D. Can MTR be used to assess cartilage in the presence of Gd-DTPA^{-2}? Magn Reson Med 2002;48:1081–1084.
39. Matsushima S, Sasaki F, Yamaura H, Iwata H, Ohsaki H, Era S, Sogami M, Inaba T, Uike M, Kinosada Y. Equivalent cross-relaxation rate imaging for sentinel lymph node biopsy in breast carcinoma. Magn Reson Med 2005;54:1300–1304.